Lawrence Berkeley Laboratory
UNIVERSITY OF CALIFORNIA, BERKELEY

EARTH SCIENCES DIVISION

To be published in the Journal of Geophysical Research

HYDROMECHANICAL BEHAVIOR OF A DEFORMABLE ROCK FRACTURE SUBJECT TO NORMAL STRESS

Y.W. Tsang and P.A. Witherspoon

January 1981

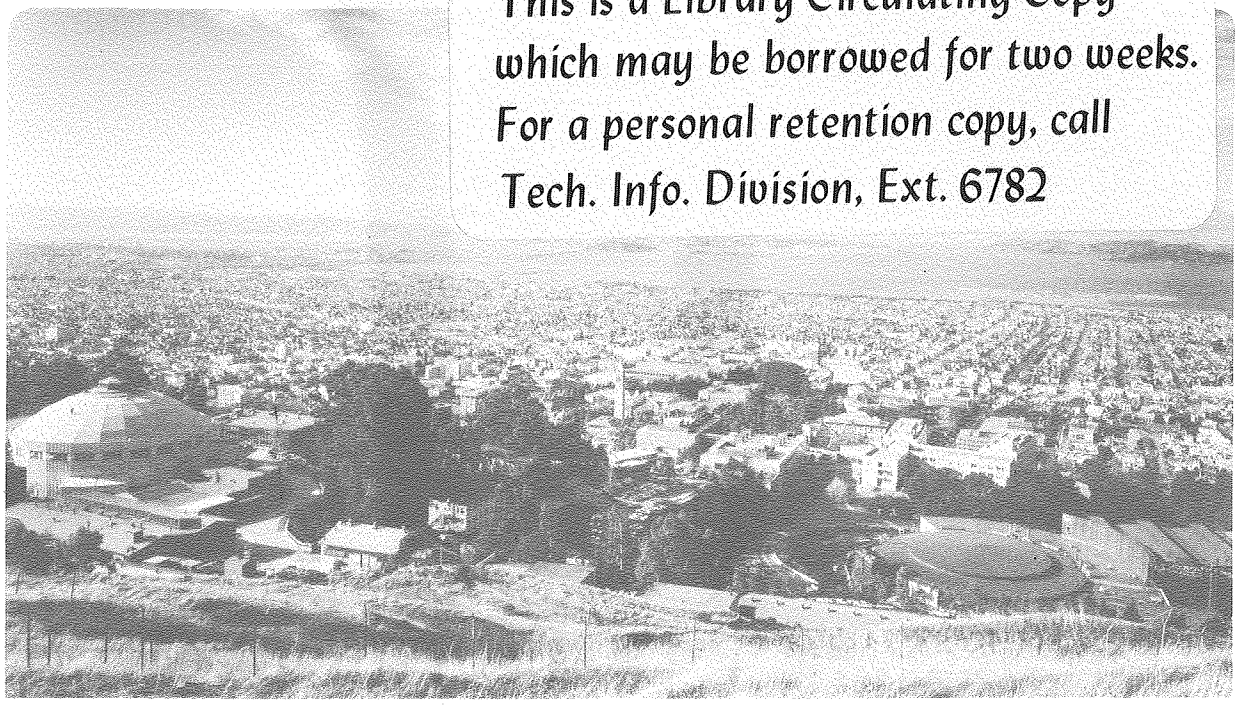

Prepared for the U.S. Department of Energy under Contract W-7405-ENG-48

DISCLAIMER

Article accepted for publication in
Journal of Geophysical Research

LBL-12297

Hydromechanical Behavior of a Deformable Rock Fracture Subject to Normal Stress

Y. W. Tsang and P. A. Witherspoon

January 1981

This work was supported by the U. S. Department of Energy under contract W-7405-ENG-48 with Lawrence Berkeley Laboratory, University of California, Berkeley, California.

ABSTRACT

A simple physical model is developed to understand the effect of normal stress on fluid flow through a single fracture. Roughness along the fracture walls plays a definite role in controlling the flow. In the usual parallel-plate representation for a fracture, the flow is proportional to the cube of the constant aperture, b. However, when the effect of fracture roughness is taken into account, the flow follows an equivalent "cubic" law where the cube of the single value for the aperture must be replaced by an appropriately weighted average $\langle b^3 \rangle$. To obtain this average value, a physical model was developed wherein the single fracture is represented by a collection of voids and the closure of the fracture results from a deformation of these voids. The model enables one to characterize the fracture roughness from a relationship between the stress-displacement measurements of intact rock and those of jointed rock. This calculated value of $\langle b^3 \rangle$ leads to flow rate as a function of normal stress. Predicted flow rates using this model are in good agreement with results from laboratory data on granite and basalt. By making several simplifying physical assumptions, we have eliminated the necessity of incorporating fitting parameters to the flow data. In this manner, a basic understanding of the factors controlling the flow of fluids through fractures has been obtained.

INTRODUCTION

This paper is an attempt to develop a basic understanding of flow through fractured rock masses that are under stress. The hydromechanical coupled system chosen for our study is a single horizontal rough-walled fracture under normal stress. Our theory

(i) relates the mechanical properties of the fractured rock to the geometrical characterization of the rough-walled fracture;

(ii) modifies the equation describing flow through a fracture with smooth parallel walls to include the effect of the roughness of the fracture surfaces; and

(iii) predicts the flow rate as a function of normal stress on the fractured rock.

Our theory is validated against laboratory experiments with radial flow through single fractures in granite and basalt cores.

Steady laminar flow of a viscous incompressible fluid in a fracture composed of two smooth, parallel walls separated by distance b obeys the cubic law, that is, the flow rate is proportional to b^3 [Boussinesq (1868), Lomize (1951), Snow (1965), Romm (1966), Bear (1972), Iwai (1976)]. In actual rock fractures the walls are far from smooth [Louis (1969), Sharp (1970), Ohnishi (1973)]. The asperities protruding into the flow stream vary in height and can be as tall as the fracture aperture b itself. In this paper we will examine the validity of the cubic flow law for flow through a rough-walled fracture. We show that an equivalent cubic law may be used as long as the "typical size of the asperity" (the typical distance over which the aperture

may be considered constant) is small compared to the scale of the flow region under study. When this physical constraint is satisfied, the effect of fracture roughness enters into the flow equation by introducing a statistical average for the variation in aperture. This implies that a rough wall fracture may be suitably modeled using a mathematical expression for aperture distribution. A schematic model of a fracture consisting of a smooth top slab and a rough bottom slab with asperities of different heights (h_j) is shown in Fig. 1. The configuration of asperities gives rise to a fracture with variable apertures (b_j).

Though an asperity model for a fracture seems to be the natural candidate for the study of fluid flow through fractures, it is not suited to the interpretation of the mechanical property of a single fracture under stress. The fact that the elastic modulus of a jointed rock is, in general, less than that of an intact rock is well established [Goodman, 1974, 1976]. Typical normal stress-displacement curves for intact rock and jointed rock are shown schematically in Fig. 2. The shapes of the slopes of these curves clearly demonstrate that at low stress (< 10 MPa) the Young's modulus for the jointed rock is much smaller than that of the intact rock. As stress increases, the modulus increases and approaches the value of the intact rock at higher stresses.

Gangi (1978) has used an asperity model to determine the stress dependence permeability in fractured rock. In Gangi's "bed of nails" model, the closure of the fracture under stress is ascribed to the elastic compression of the asperities, and the "softness" of the fracture is said to result from the small

number of asperities that are in contact. These contact areas therefore sustain much higher stresses than that measured by the total load divided by the total fracture area. As a result, the strain of the asperities in contact is expected to be larger than the strain in the intact rock under the same load. With this "bed of nails" model, Gangi obtained a very good fit to flow data for a fractured sandstone [Nelson, 1975].

However, when we applied such a model to both the flow data and stress-strain measurements for a granite fracture [Iwai, 1976], we encountered some difficulty. Equations used in our analysis are given in the Appendix. We found that in order to obtain a result that was quantitatively compatible with Iwai's flow data, we arrived at a contact area that, at the maximum experimental stress level of 20 MPa, was only 0.001 of the total fracture area. In contrast, Iwai's experimental results for contact area at this maximum stress were between 0.1 and 0.2. This discrepancy between theory and measurement is too large to be ignored. Furthermore, when we required the theoretical fractional contact area to conform to Iwai's (1976) measured values, then no agreement between calculated and measured flow rates could be obtained. To force an agreement required adopting a value of Young's Modulus for each asperity that was two orders of magnitude smaller than that of intact rock, which does not seem reasonable. We therefore proceeded to seek an alternative physical model for the hydromechanical behavior of a single fracture under normal stress.

In this present study, we consider the closure of a fracture as resulting from the deformation of "voids" or "cracks" between the asperities. The

physics of this void model predicts a very soft elastic property at low stresses; it also predicts a gradual increase of the effective Young's modulus to approach the intrinsic value of solid rock, in accordance with the behavior displayed in Fig. 2. Geometrically, one may either envision a single fracture as composed of a collection of voids or a distribution of asperities as illustrated in Fig. 3. The asperity model and the void model are entirely interchangeable as far as the geometry of the fracture is concerned.

Our theory utilizes the void model to describe the behavior of the fracture under normal stress and the asperity model to describe the flow through a rough-walled fracture. A mathematical correspondence between the void model and asperity model is developed. This correspondence allows the prediction of the flow rate as a function of normal stress. As no arbitrary adjustable parameter is employed in the validation of this theory, our model probably contains the essential physics relevant to the problem of fluid flow through a single fracture under normal stress.

GEOMETRICAL CHARACTERIZATION OF FRACTURE ROUGHNESS FROM ELASTIC PROPERTIES

From the slopes of the normal stress-displacement curves such as those shown in Fig. 2, one can obtain the intrinsic Young's modulus E for the solid rock and the effective Young's modulus E_{eff} for the jointed rock from

$$E(\sigma, \Delta V_r) = \ell \frac{d\sigma}{d\Delta V_r}$$

$$E_{eff}(\sigma, \Delta V_t) = \ell \frac{d\sigma}{d\Delta V_t} \qquad (1)$$

(See nomenclature for definitions of terms.)

At low stresses, the effective Young's modulus E_{eff} of the jointed rock is much smaller than that of the solid rock. As stress is increased, E_{eff} approaches the value of E for the solid rock. This behavior can be successfully reproduced if the single fracture of the jointed rock is modeled as a collection of voids.

Consider first the geometry of one elliptic flat crack of length 2d enclosed in a rock volume of $u = \Delta x \Delta y \Delta z$. Following closely the formulation of Walsh (1965), one can show that for a rock with a collection of voids, all with the same orientation as the one shown in Fig. 4, the effective modulus E_{eff} of the rock with voids is related to the intrinsic rock modulus E by

$$\frac{1}{E_{eff}} = \frac{1}{E} + \frac{4\pi \langle d^3 \rangle}{E \langle u \rangle} , \qquad (2)$$

where both the crack length cubed and the volume enclosing each void have been averaged over all the voids in the sample. This expression is not sensitve to the actual shape of the void. Walsh's derivation involved the determination of the strain energy of a rock mass containing no voids and the increase in strain energy due to the presence of voids. The second term on the right-hand side of (2) arises from the strain energy associated with the cracks. Since (2) applies to a physical situation of sparse voids, the effect of the voids on the elastic modulus is expected to be small. Then the property of the rock medium in which the voids are situated may be described by Young's modulus for intact rock, and therefore the same modulus E appears in the strain energy term associated with the cracks.

Let us now consider one single horizontal fracture as a collection of voids and translate the geometry of one flat crack in Fig. 4 to the situation in Fig. 5. Here the voids are dense and the void ratio is large. Only a small fraction of the total fracture area is in contact. To describe the effective modulus E_{eff} of the fractured rock in the vicinity of the fracture, (2) may be modified to

$$\frac{1}{E_{eff}} = \frac{1}{E} + \frac{4\pi \langle d^3 \rangle}{E_{eff} \langle u \rangle} , \tag{3}$$

where (3) now includes E_{eff} in the last term. When the voids are large in number and close in proximity, the void-void interaction is no longer negligible as is assumed in the derivation of (2). Since it is difficult if not impossible to account for this interaction in the calculation of strain energies, we make a plausibility argument to lump the effect of the interaction by introducing E_{eff} in the last term of (3). The argument being that due to the high void ratio, the property of the rock medium is better represented by the effective modulus of the fractured rock than by the modulus of the intact rock. Equation 2 is the weak interaction limit when void ratio is small and (3) is the intermediate interaction range when void ratio is large in the calculation of the effect of voids on the elastic moduli of rocks.

Suppose there are M voids in the fracture with a total cross sectional area A. Then the average volume enclosing each crack may be written as

$$\langle u \rangle = \frac{A \Delta z}{M} \tag{4}$$

where Δz is a thickness around the fracture within which E_{eff} is applicable (see Fig. 5). Since the rock fracture is represented by a collection of voids, one expects the contact area of the fracture walls to be small such that the total void area is almost identical to the total fracture cross section area A. Therefore,

$$\langle (2d)^2 \rangle_M \approx A \ . \tag{5}$$

In addition, for a spatially random collection of M voids, $\langle d^3 \rangle \approx \langle d^2 \rangle \langle d \rangle$, (3) may now be written approximately as

$$\frac{E_{eff}}{E} = 1 - \frac{4\pi \langle d^3 \rangle}{\bar{u}} \approx 1 - \frac{\pi M \langle (2d)^2 \rangle \langle d \rangle}{A \Delta z} \approx 1 - \frac{\pi \langle d \rangle}{\Delta z} \ . \tag{6}$$

An actual calculation using random numbers showed that $\langle d^3 \rangle$ is about one and a half times that of $\langle d^2 \rangle \langle d \rangle$. The approximation that they are equal, together with the approximation in (5) will introduce a numerical constant in the last term of (6). It will be clear from the discussion following (8) that whether this constant is one as shown in (6) or otherwise will have absolutely no effect in all the results derived from the physical model proposed here. Note that (6) gives the impossible result of negative E_{eff} if $\langle d \rangle > \Delta z/\pi$. Very large $\langle d \rangle$ corresponds to the physical limit of a fracture with no contact area, which is the strong interaction limit of the physical model. This limit is not described properly by (3) from which (6) is deduced.

The physical picture implied by (6) is illustrated schematically in Fig. 6, which is an attempt to portray a portion of fracture shown in Fig. 5 at different stages of normal stress. The crack length 2d is defined as the distance between two adjacent areas where the two fracture surfaces come into

contact. These areas of contact are simply the asperities as shown in Fig. 3. Under increasing load, the deformation of the voids causes more asperities to come in contact, and leads to a decrease in the average crack length. This process results in a gradual increase of the effective modulus with increasing normal stress according to (6). The average crack length $2\langle d \rangle$ continues to decrease as the voids deform until the term $\pi\langle d \rangle/\Delta z$ becomes negligibly small compared to 1, at which point the jointed rock will exhibit an effective modulus identical to that of the intrinsic modulus. Recall that Δz is the thickness around the horizontal fracture where the rock must be characterized by the effective modulus. For a fracture with a maximum aperture at zero stress of a few hundred microns (10^{-2} cm), one might conjecture Δz to be on the order of centimeters. With such a rough estimation of Δz in eq. (6), one can show that when the average crack length decreases to the order of a few microns, the effective modulus differs from the intrinsic value of intact rock by no more than 1%.

We emphasize that when the Young's modulus exhibited by a jointed rock is very much smaller than that of intact rock (one to two orders of magnitude at low stresses as reported by Iwai, 1976), the "softness" of the jointed rock must be interpreted as caused by the deformation of the voids surrounded by contact areas and not due to the elastic compression of the asperities. However, in the case of a "stiffer" joint, where Young's modulus of the discontinuous rock is not too different from that of intact rock, then the attribution of the fracture displacement to the compression of asperities should be valid. However, at low stress when the fracture closes easily, then deformation of voids is proposed as the controlling mechanism.

Our discussion so far does not exclude the possibility of inelastic crushing of the asperities in the process of loading, this point will be discussed below. It is clear from Fig. 6 that one may view the sequence (a) (b) (c) either as a decrease in the average crack length $2\langle d\rangle$ or as an increase in the number N_c of areas in contact under increasing load. For a rough-walled fracture, we shall describe the former process as a "void model" and the latter process as an "asperity model." For a spatially random distribution of voids or asperities, N_c varies inversely with $\langle d\rangle$. Given elastic stress measurements, it is evident from (6) that the relative average crack length $2\langle d\rangle$ as a function of stress or fracture displacement can be calculated, and in turn, N_c may be deduced.

The number of contact areas, N_c, is the key to aperture distribution. Fig. 1 represents a rough-walled fracture as an array of asperities of varying heights h_j and corresponding aperture b_j. At zero applied stress, the maximum possible aperture is b_o. With applied axial stress σ, the fracture closure ΔV results in a downward displacement of the top slab. At nonzero stresses, the aperture which corresponds to each asperity of height h is

$$b = \begin{cases} (b_o - \Delta V - h) & h < (b_o - \Delta V) \\ 0 & h \geq (b_o - \Delta V) \end{cases} \tag{7}$$

Let n(h) denote the asperity height frequency distribution function which characterizes the fracture prior to loading. Then N_c, the total number of asperities in contact at any stress, is

$$N_c(\Delta V) = \int_{b_o - \Delta V}^{b_o} n(h)dh. \tag{8}$$

It is clear from (8) that the asperity height distribution function, n(h), can be obtained from the derivative of N_c.

For a given set of stress-displacement measurements, it is possible only to deduce the change in $\langle d \rangle / \Delta z$ relative to its value at zero applied stress from (6). This implies that N_c and in turn n(h) can only be determined to within some constant multiplier. However, if one knows the approximate percentage of the contact area at a particular stress, then this constant can be determined without ambiguity. Once n(h) is obtained, the aperture distribution is also known since aperture is related to asperity height by (7).

To recapitulate, stress-displacement measurement of fractured and unjointed rock can be used to derive the relative average crack length and in turn the relative number of asperities in contact. This provides a bridge between the "void" model and the "asperity" model. One can then correlate the elastic stress displacement measurements in jointed rock to the geometrical characterization of the roughness of the fracture surfaces. The actual calculation of $2\langle d \rangle$, N_c and n(h) will be presented below.

EQUIVALENT CUBIC FLOW LAW FOR A ROUGH-WALLED FRACTURE

We now turn to the derivation of an appropriate expression for flow through a rough-walled fracture. It has been shown [Boussinesq (1868), Lomize (1951), Snow (1965), Romm (1966), Bear (1972)] that steady laminar velocity of a viscous incompressible fluid through a fracture composed of two smooth parallel walls separated by distance b satisfies the equation

$$\vec{V} = - \frac{\rho g}{12\mu} b^2 \nabla \vec{H}. \tag{9}$$

Note that (9), which governs the flow through a fracture bounded by two flat, parallel plates, has the same form as Darcy's law for porous isotropic media. In both cases b is a constant throughout the medium. It follows from (9) that the volumetric flow obeys the cubic law, namely

$$\frac{Q}{\Delta H} = Cb^3 \tag{10}$$

where C is a proportionality constant that depends on the geometry of the system and properties of the fluid. For straight flow through a rectangular sample of length L and width W

$$C = - \frac{W}{L} \frac{\rho g}{12\mu} . \tag{11}$$

For radial flow in a cylindrical sample of radius r_e and wellbore radius r_w,

$$C = - \frac{2\pi}{\ell n \frac{r_e}{r_w}} \frac{\rho g}{12\mu}. \tag{12}$$

In actual rock fractures, the fracture walls are far from smooth and the question of the validity of (9) and (10) therefore arises. In a recent analysis of results of laboratory investigations on flow through rough fractures, Witherspoon et al. (1980) have found the cubic law to hold. The effect of roughness causes a reduction in flow from that predicted using (10). However, this flow reduction can be handled through an empirical multiplication factor to the constant C in (10) without altering the cubic dependence on fracture opening.

Let us now examine the theoretical validity of the cubic law for steady laminar flow through a rough-walled fracture. Consider two-dimensional flow within a horizontal fracture in the x-y plane (r-θ plane in cylindrical coordinates). The fluid velocity $\vec{V}(x, y)$ referred to in the following is an average over the z direction, that is, over the fracture aperture. The roughness in the fracture walls is represented by the aperture function b(x, y). For flow through a rough-walled fracture of variable aperture, (9) may be rewritten for any point (x, y)

$$\vec{V}(x, y) = - \frac{\rho g}{12\mu} b^2(x, y)\nabla\vec{H}, \tag{13}$$

furthermore, for incompressible, steady flow,

$$\vec{\nabla} \cdot \nabla = 0. \tag{14}$$

Equations 13 and 14 give

$$\nabla \cdot \left(- \frac{\rho g}{12\mu} b^2(x, y)\nabla\vec{H} \right) = 0. \tag{15}$$

This equation generally cannot be solved analytically for an arbitrary b(x, y).

If one sacrifices mathematical rigor and makes some further assumptions based on the physics of the problem, a useful expression can be developed. Consider the fluid flow in a single horizontal fracture in the x-y plane with a pressure head maintained between x = 0 and x = L. Fig. 1 shows a schematic model for the cross section of a fracture with variable aperture. It can serve as a model for the x-dependence of b(x, y) at a fixed y, or the y-dependence of b(x, y) at a fixed x, depending on whether the cross section considered is perpendicular to $\hat{y}$ axis or $\hat{x}$ axis, respectively. We shall term the a_j's in

Fig. 1 the "asperity length" because they are the lengths over which the aperture may be considered to be constant and take on the value b_j. Aperture b_3 in Fig. 1 is explicitly allowed to vanish over the length a_3 to simulate the situation in real fractures where there exist areas of contact over which the fracture is closed. Keeping in mind that a pressure gradient is maintained along the $\hat{x}$ axis, it is clear from the schematic model in Fig. 1 that when the fluid flow is averaged over a length segment that is large by comparison with the scale of a_j, the flow is essentially in the $\hat{x}$ direction. The fluid velocity does, of course, have a $\hat{y}$ component for dimensions that are on the order of a_j in magnitude. In other words, as long as the typical size of the asperity is small in comparison with the scale of the macroscopic dimensions of the sample, it is permissible to assume the fluid velocity to have only an $\hat{x}$ component. For any cross section at a fixed $\hat{x}$ coordinate x_o, the macroscopic average velocity is therefore:

$$\vec{V}(x_o, y) = \hat{x}V(x_o, y) = -\hat{x}\,\frac{\rho g}{12\mu}\,b^2(x_o, y)\,\left.\frac{dH}{dx}\right|_{x_o} . \tag{16}$$

The total average flow through the width W, at x_o is

$$Q(x_o) = \int_0^W V(x_o, y)b(x_o, y)\,dy$$

$$= -\frac{\rho g}{12\mu}\left.\frac{dH}{dx}\right|_{x_o} \int_0^W b^3(x_o, y)\,dy$$

$$= -\frac{\rho g}{12\mu}\left.\frac{dH}{dx}\right|_{x_o} \sum_j a_j b_j^3$$

$$= - \frac{\rho g}{12\mu} \left.\frac{dH}{dx}\right|_{x_o} W\langle b^3\rangle_{x_o} \tag{17}$$

where $\langle b^3\rangle$ is by definition the weighted average:

$$\langle b^3\rangle = \frac{\sum_j a_j b_j^3}{\sum_j a_j} = \frac{\sum_j a_j b_j^3}{W} . \tag{18}$$

Equation 17 is the cubic flow law at a fixed x_o for a fracture whose variation in aperture is transverse to the average flow. The total flow through the cross section at this fixed x_o is equivalent to a uniform aperture of $\langle b^3(x_o, y)\rangle_{x_o}^{1/3}$. We now consider the variation of the aperture longitudinal to the average flow, that is, consider a cross section at a fixed y coordinate, y_o. Equation 13 gives

$$\vec{V}(x, y_o) = -\hat{x} \frac{\rho g}{12\mu} b^2(x, y_o) \left.\frac{dH}{dx}\right|_{y_o} \tag{19}$$

and $\nabla \cdot \vec{V} = 0$ implies

$$- \frac{\rho g b^2(x, y_o)}{12\mu} \left.\frac{dH}{dx}\right|_{y_o} = U \tag{20}$$

U is a constant independent of x, it is related to the flow at any x by

$$U = - \frac{Q(x)}{W\langle b^3\rangle_x^{1/3}} . \tag{21}$$

Summing the pressure drops along the length of the sample:

$$\int_0^L dH(x) = \int_0^L \frac{-12U\mu}{\rho g b^2(x, y_o)} dx$$

$$= \frac{-12U\mu}{\rho g} \sum \frac{a_j}{b_j^2}$$

$$= -12 \frac{U\mu L}{\rho g} \left\langle \frac{1}{b^2} \right\rangle_{y_o} \tag{22}$$

(21) and (22) lead to the flow in a variable-width fracture:

$$Q(x) = \frac{W}{L} \frac{\rho g}{12\mu} \langle b^3 \rangle_x^{1/3} \frac{1}{\left\langle \frac{1}{b^2} \right\rangle_y} [H(0) - H(x)] \tag{23}$$

where $\langle b^3 \rangle_x^{1/3}$ is an average over the width of the sample, it arises from the variation of aperture transverse to the macroscopic flow; $\langle 1/b^2 \rangle_y$ is an average over the length of the sample, it arises from the aperture variation longitudinal to the macroscopic fluid flow. Equation 23 differs from the parallel-plate description of a smooth fracture [(10) and (11)] in that two statistical averages of the variable aperture now replace the constant aperture-cubed term.

Following the procedure of the derivation above, we can show that for divergent radial flow in a cylindrical rock sample of radius r_e and wellbore radius r_w, an expression corresponding to (23) may be derived:

$$Q(r_e) = \frac{-2\pi}{f \ln \frac{r_e}{r_w}} \frac{\rho g}{12\mu} \langle b^3 \rangle_r^{1/3} \frac{1}{\left\langle \frac{1}{b^2} \right\rangle_\theta} [H(r_w) - H(r_e)] \tag{24}$$

Here, $\langle b^3 \rangle_r^{1/3}$ arises from the average over the variation of aperture transverse to the macroscopic radial flow and $\langle 1/b^2 \rangle_\theta$ arises from the average over

the variation of aperture longitudinal to the radial flow direction. The presence of the numerical factor f ($f \geq 1$ and varies with the ratio r_e/r_w) in addition to the usual geometrical factor associated with radial flow in (12) is a correction for size-effect in the case of cylindrical symmetry. This correction factor emerges from consideration of the variation of fracture width longitudinal to the radial flow direction. The derivation is similar to that outlined in (19) through (22), but when the summation in (22) is carried out numerically for different ratios of r_e/r_w, the geometrical factor $f \ln(r_e/r_w)$ results. Calculated values of f are tabulated in Table 1 to show that the correction becomes negligible as the ratio r_e/r_w becomes large. On the other hand, these results indicate that for rock samples whose dimensions are such that the outer radius is less than seven times the wellbore radius, the assumption that flow is radial is probably a poor approximation.

Table 1. Size effect correction factor for radial flow.

r_e/r_w	f
7	1.093
13	1.033
37	1.008
61	1.004

CALCULATION OF FRACTURE FLOW AS A FUNCTION OF STRESS

From (6), (7), and (8), we have shown that stress-displacement measurements for fractured rock can be used to arrive at aperture functions for different values of normal stress. Furthermore, (23) and (24) indicate that when a fracture can be characterized by an aperture function, a statistical averaging of the variation in aperture over the entire fracture may be carried out to obtain the fluid flow. In the following, we shall consider the application of this theory to specific cases where experimental measurements are available.

Iwai (1976) performed laboratory investigations on the mechanical and hydrological properties of tension fractures in samples of basalt, granite, and marble. Cylindrical samples of intact rock, 0.15 m in diameter, were diamond-cored from blocks, and a horizontal tension fracture was created in each sample using a modified form of the "Brazilian" loading method [Goodman, 1974]. A center hole, 0.022 m in diameter, provided access for outward radial flow of water. Three LVDT's (linear variable differential transformers) placed 120° apart and mounted so as to straddle the fracture were capable of detecting aperture changes as small as 0.4 μm. Elastic deformation measurements of the intact rock were performed on solid samples diamond-cored from the same rock block. Iwai's data for the mechanical properties of granite, basalt, and marble are shown in Figures 7, 8, and 9, respectively. The labels $\Delta V_{t,1}$, $\Delta V_{t,2}$, $\Delta V_{t,3}$ refer to measurements recorded by the LVDT's, from which an average value, ΔV_t was determined. The fracture deformation, ΔV, was obtained by subtracting the rock deformation, ΔV_r, from ΔV_t. Deformations were measured with water flowing through the horizontal fracture.

To determine the aperture distributions, analytic functions were fitted to the stress displacement data in Figures 7-9. The effective and intrinsic Young's moduli for each material at different stages of stress were computed from the derivative of these functions, using (1). Equation 6 was then used to obtain the relative crack length $2\langle d \rangle$. N_c, the total number of asperities in contact as a function of fracture closure, followed since it is inversely proportional to $2\langle d \rangle$. The results are plotted as points in Fig. 10, and analytic functions, represented by the solid lines were fitted to these points. The asperity height distribution function n(h) was then computed using (8), from which we evaluated the aperture averages in (23) and (24).

A further assumption was necessary to simplify the actual computations. In a real fracture, the variation of the aperture is expected to be spatially random, and thus, the same set of aperture frequency distributions should be applicable to a description of the fracture regardless of the orientation of the cross section chosen. Therefore, the subscripts x, y, r, and θ in the statistical averages in (23) and (24) may be dropped. Furthermore, if the average macroscopic flow is in fact along x, the average of $\langle b^3 \rangle_x$ in (23) may be carried out first, giving an effective fracture opening of $\langle b^3 \rangle_x^{1/3}$; then the subsequent average $\langle 1/b^2 \rangle_y$ is trivial:

$$\frac{1}{\left\langle \frac{1}{b^2} \right\rangle_y} = \frac{1}{\left\langle \frac{1}{\langle b^3 \rangle_x^{2/3}} \right\rangle_y} = \langle b^3 \rangle^{2/3}. \qquad (25)$$

Equation 23 then reduces to

$$Q(x) = -\frac{W}{L}\frac{\rho g}{12\mu}\langle b^3\rangle(H(0) - H(x)). \tag{26}$$

for straight flow geometry, and (24) reduces to

$$Q(r_e) = -\frac{2\pi}{f\,\ell n\left(\frac{r_e}{r_w}\right)}\frac{\rho g}{12\mu}\langle b^3\rangle[H(r_w) - H(r_e)] \tag{27}$$

for radial flow.

The statistical average for the variation in aperture was computed from:

$$\langle b^3(\Delta V, \sigma)\rangle = \frac{\int_0^{b_o-\Delta V}(b_o - \Delta V - h)^3 n(h)\,dh}{\int_0^{b_o} n(h)dh}. \tag{28}$$

The maximum aperture, b_o, of the fracture at zero stress can be determined from the contact area at a specified stress. If the contact area as a fraction of the total fracture area is known to be ω at a specified deformation ΔV, then

$$\omega = \frac{N_c(\Delta V)}{N_c(b_o)} \tag{29}$$

because by definition, the fracture will be totally closed when $\Delta V = b_o$. From (29), b_o is readily determined.

It is implicit in (28) and (29) that all asperities have the same cross-sectional area. This assumption is physical. The size of each asperity should be on the order of a, the typical "size of the asperity" discussed

above. Then $N_c(b_o)$ multiplied by a^2 simply gives A, the total fracture cross-sectional area. Our choice of the functional form of $N_c(\Delta V)$ to fit the calculated values was governed by two considerations: (i) $N_c(\Delta V)$ is an increasing function of ΔV, and (ii) n(h) the derivative of $N_c(\Delta V)$, is such that the integral in (28) may be carried out analytically. The latter constraint considerably limited the range of our choice. We settled on a power functional dependence for $N_c(\Delta V)$ given by:

$$N_c(\Delta V) = N_c(0) + \alpha(\Delta V)^{\beta} \tag{30}$$

and

$$n(h) = \alpha\beta(b_o - h)^{\beta-1} \tag{31}$$

where $N_c(0)$, α and β were the fitting parameters to be derived from the calculated values of of $N_c(\Delta V)$. Note that according to (8), n(h) is only defined from $N_c(\Delta V)$ for $h \geq (b_o - \Delta V)$, whereas the statistical average in (28) requires the entire range of n(h) from zero through b_o. The functional form in (31), therefore, supplies the extrapolated values of n(h) in the interval $0 \leq h < (b_o - \Delta V_m)$ where ΔV_m is the maximum value of the measured fracture closure. After calculating average apertures from (28), radial flow as a function of stress could be obtained using (27).

Iwai estimated ω, the fraction of contact area in the single fracture, by a method similar to that of an impressograph. He found the value of ω to be 0.1-0.2 for granite and 0.25-0.35 for marble at a normal stress of 20 MPa. No measurements of ω for basalt were reported. We used the range of values ω = 0.1, 0.15, 0.2 for both granite and basalt, and the value 0.25 for marble in the calculation of flow as a function of normal stress, $Q(\sigma)$. Results of

calculated flow versus stress are compared to experimental data for granite, basalt, and marble in Figures 11, 12, and 13, respectively. The effects of variations in ω are included in Figures 11 and 12. Recalling that no arbitrary adjustable parameter was involved in the calculation, we consider the agreement, between the calculated theoretical flow and the measurements, in the cases of granite and basalt to be remarkable. In the case of marble the agreement between theory and measurements is poor. An explanation for this will be given in the following section.

Iwai (1976) also studied the effect of repeated loading on the mechanical and flow behavior of a fracture. In the case of basalt, very little hysteresis in the stress-displacement data was observed. Whereas in the case of granite, there was a considerable amount of permanent set as shown in Fig. 14. The difference can be understood in terms of fracture roughness profiles between basalt and granite. The fracture roughness profile was modeled by $N_c(\Delta V)$, as derived from the stress-displacement data of the first loading cycle. The function $N_c(\Delta V)$ in Fig. 10 can be converted to a fracture profile in real space in terms of separation between asperities and asperity heights; a small portion of such a profile including two asperities of maximum height b_o is shown in Fig. 15. Since our theory only determines the relative crack length but not the absolute crack length, the horizontal scale is left in arbitrary units. However, for a physically realistic crack length on the order of a centimeter at zero stress, the horizontal scale should be expanded about 50 times in order to conform to the same unit as the vertical scale. It is clear from Fig. 15 that the granite fracture surface includes a few asperities that are much taller than the rest. It is very likely that these

asperities would be crushed by repeated loading, giving rise to a permanent set. By comparison, the asperity heights of the basalt are relatively more "uniform" so that the crushing of tall asperities is less probable. Since the crushing of tall asperities in a fracture under repeated loading changes the roughness profile of the fracture, one should expect the flow rate as a function of stress to be different after several cycles. Such an interpretation is supported by Iwai's (1976) flow data for granite and basalt after repeated loadings. His results for flow versus stress differ substantially from cycle to cycle in granite whereas the flow remains essentially the same with repeated loading in basalt.

Theoretical calculations to predict the flow for the different loading and unloading cycles in granite were carried out in the same manner as discussed earlier. Beginning with the stress-displacement data for granite in Fig. 14, we calculated the function for the asperities in contact and derived the theoretical flow $Q(\sigma)$ for each cycle separately. The theoretical predictions as compared to data are shown in Figs. 16 and 17. The fractional contact area was assumed to be 0.15 in all calculations. Similar calculations were not carried out for basalt because the differences in the flow data for different cycles were too small to render a meaningful comparison between data and our theory. Relevant parameters used in equation 31 for all cases calculated so far are tabulated in Table 2.

Table 2. Selected parameters used in the "void" model.

Rock type and mechanical specification	ω	β	b_o (μm)	ΔV_m (μm)
granite, run 1, loading	.15	35.	114.44	108.20
granite, run 1, unloading	.15	36.	114.54	108.20
granite, run 2, loading	.15	13.	41.32	35.37
granite, run 2, unloading	.15	14.5	40.92	35.37
basalt, run 1, loading	.15	7.5	65.78	49.50
marble, run 1, loading	.25	15.	37.22	33.80

DISCUSSION OF RESULTS

Since our present theory involves no flow data fitting, the agreement between theory and flow data displayed in Figs. 11, 12, 16, and 17 has some important implications. It indicates that our theory probably contains the essential physics that is relevant to the problem of fracture flow coupled with stress. The theory contains several simplifying assumptions, but it does not depend on an arbitrary adjustable parameter. The lack of any fitting parameters in the interpretation of flow versus stress data is the key difference between this work and previous studies [Gangi (1978), Witherspoon et al. (1980)]. Our physical theory requires the input of (i) the stress-displacement data for both the unjointed and jointed rock, and (ii) an estimated fractional contact area for the fracture walls at a specified stress. The stress-displacement data lead to the derivation of the relative asperity-height distribution. The fractional contact area supplies the constant which allows

the calculation of the absolute height of the tallest asperity. The salient feature of the theory is that a roughness profile of the fracture may be deduced from the stress-displacement measurements, which in turn allows the prediction of flow as a function of stress.

In general, any or all of the several physical assumptions and mathematical approximations in our model can contribute to errors in the calculated result for flow. In particular, $N_c(\Delta V)$, the number of asperities in the contact function, and n(h), the asperity height distribution function, are involved in all phases of the computation; it is likely then that errors associated with these quantities may play a greater role in contributing to the discrepancy between the theoretical prediction of flow and the experimental measurements. Recall that the mathematical treatment of $N_c(\Delta V)$ and n(h), involved the following: (i) the fitting of an analytic function to the stress-displacement data. (ii) the fitting of an analytic function to the calculated values of $N_c(\Delta V)$, and (iii) the definition of the values of n(h) in the range of small h by extrapolation from the analytic function fitted to $N_c(\Delta V)$. It is clear that these various manipulations can all contribute to error in the subsequent prediction of the theoretical flow $Q(\sigma)$.

Figure 10 shows that an exact fit to the calculated values of $N_c(\Delta V)$ by the analytic function (30) is not obtained with all three rock types. This would account for some discrepancy in the theoretical flow and in the data (Figs. 11, 12, 13). In treating the stress-displacement data in order to calculate $N_c(\Delta V)$, we encountered no difficulty in choosing an analytic function with an excellent fit in the cases of granite and basalt (Figs. 7 and 8).

However, the stress-displacement data for marble (Fig. 9) could not be fitted by an analytic function throughout the range of measured stress due to the "anomalous" shape of the data (note in particular the component $\Delta V_{t,1}$ in Fig. 9). The analytic function chosen deviated significantly from the measured ΔV_t for stresses greater than 2 MPa. Since the values of $N_c(\Delta V)$ are calculated from the derivatives of stress-displacement curves, the effect of any discrepancy in the theoretical fit to the stress-displacement data would be greatly magnified in the resultant $N_c(\Delta V)$ values. Therefore, the resultant $N_c(\Delta V)$ for marble is probably a poor representation of the actual roughness profile of the fracture walls, thus giving rise to errors in the prediction of flow (Fig. 13). Furthermore, the nonsmoothness of the theoretical flow curve in Fig. 13 is further evidence of noise in the stress-displacement data for marble. Of course, one may choose to fit the stress-displacement data numerically rather than by an analytic function which will require numerical integration of (28). It is conceivable that such a procedure could produce a better fit to the resultant flow. However, since it is not clear whether the anomaly in the stress-displacement data as shown in Fig. 9 was actually physical or experimental in nature, and since the emphasis of this present study is on the understanding of the physical processes rather than the exact fitting of curves, we did not pursue this matter further, but devoted our efforts to calculations on granite and basalt. Finally, the use of extrapolated values for n(h) in the range of h from 0 to $(b_o - \Delta V_m)$ introduces error in the theoretical calculation of flow, especially in the region of high stresses. However, the significance of the error introduced by this approximation can only be assessed after our theory is compared with much more data.

It appears then that given relatively noise-free stress displacement data, our theory can predict flow behavior in reasonable agreement with measurements. Both a "void" and an "asperity" description of the fractures were used in the theory. The former is suited to the mechanical property and the latter to the hydrological property of the rough-walled fracture. The physical picture that emerges from such a model is that at zero applied stress, the fracture is propped open by only a few tall asperities, giving rise to very long average "crack" lengths, therefore the elastic property of the jointed rock appears to be extremely soft at low applied stresses. At higher stresses, the number of asperities in contact increases rapidly, causing a rapid decrease in the average crack length, thus the Young's modulus of the jointed rock approaches that of the intact rock.

The fact that the fractional contact area at the maximum applied stress of 20 MPa is on the order of 0.15 is of interest. While the stress-displacement measurements indicate that the Young's modulus of the jointed rock becomes almost identical to that of the intact rock at this stress level, the fracture is far from being "closed"; only about 15% of the fracture surfaces are in contact. The mechanical property of the fracture becomes indistinguishable from that of the intact rock, not because the fracture is "closed," but because the average crack length under increased load has shortened sufficiently, causing the voids in the fracture to deform from elongated shapes (Figs. 4 and 5) to voids more like spheroids. Thus, with respect to its elastic property, the fracture behaves very much like an intact rock; but with respect to its hydraulic property, the fracture is definitely "open" to allow fluid transport.

Our observation therefore indicates that a fracture probably cannot be "closed" sufficiently to completely prevent hydraulic flow unless it is subjected to very high normal stresses. This seems to be consistent with the observation of Kranz et al. (1979) from their measurement of permeability from pulse decay data. Kranz et al. deduced indirectly from their data that the difference in the flow rate between a rock with and without a joint does not vanish until the effective pressure is at least 200-300 MPa.

CONCLUSION

Our investigation shows that the simple smooth parallel plate representation of a rock fracture is probably inadequate in analyzing flow through a fracture that is deforming under stress. Roughness in the fracture walls plays a definite role in affecting the flow. In the parallel-plate model for a fracture, the flow is proportional to the fracture aperture cubed. When the effect of roughness in the fracture walls is taken into account, the flow still follows an equivalent "cubic" law with the single value for the aperture replaced by a statistical average. Furthermore, in radial flow geometry, an additional correction factor due to rock sample size also arises. The correction factor developed here suggests that flow measurements performed on rock samples with sample diameter over well bore ratio that is much smaller than 7 will probably give results significantly different from measurements performed on larger samples.

In this study, we included the effect of fracture roughness in a physical model, from which flow through the fracture as a function of stress was calculated. Given the stress-displacement data (for both fractured and unjointed

rock) and the approximate fractional contact area at any specified stress, we have developed a procedure for determining roughness profiles of fractures at different levels of stress. One interesting observation from this study is that the fracture probably cannot be "closed" completely unless the applied normal stress is extremely high. In developing this model, we have made several simplifying assumptions, with the main objective of eliminating arbitrary adjustable parameters from the theory. The success in interpreting different aspects of available data on granite and basalt seems to indicate that the model is physically sound. The physical insight gained in this study is significant. It is now possible to understand how the roughness profile of a fracture changes with the application of normal stress; one can also predict the resultant flow through the fracture since it is mainly governed by the geometry of this profile. In future work, we hope to extend the concept developed here to apply to fractures under normal plus shear stresses and to networks of fractures.

APPENDIX

Figure 1 shows a schematic representation of a fracture as proposed by Gangi (1978). The asperities are indexed by j. At zero applied normal stress, each asperity is defined by height h_j, width a_j, and the corresponding aperture b_j, b_o being the maximum aperture. Assume that the asperities obey Hook's law as the top surface of the fracture in Figure 1 displaces downward by ΔV under normal applied stress, then the measured stress is:

$$\sigma(\Delta V) = \frac{1}{A} \sum_{j}' n(h_j) k_j [h_j - (b_o - \Delta V)] \tag{A1}$$

where k_j is the spring constant of the j^{th} asperity, $n(h_j)$ is the number of asperities with height h_j and the summation sums only over the asperities whose heights at zero applied stress are greater than $(b_o - \Delta V)$. To a first approximation, the spring constant may be expressed in terms of the intact rock Young's modulus E, the asperity height, and the asperity cross-section area $s_j \approx a_j^2$,

$$k_j = E \frac{s_j}{h_j} . \tag{A2}$$

Putting (A2) into (A1) and in the limit that the summation may be written as an integral, we obtain

$$\sigma(\Delta V) = \frac{E}{A} \int_{b_o}^{b_o - \Delta V} \frac{n(h)s(h)(h - b_o + \Delta V)}{h} dh. \tag{A3}$$

Therefore the variable aperture of the fracture is characterized by the asperity height and area distribution function n(h)s(h), which should satisfy the normalization condition

$$\int_0^{\Delta V} n(h)s(h) = A. \tag{A4}$$

Since the asperity height, h, and the aperture, b, at zero applied stress are related by

$$b = b_o - h \tag{A5}$$

(A3) may also be rewritten as

$$\sigma(\Delta V) = \frac{E}{A} \int_0^{\Delta V} \frac{n(b)s(b)(\Delta V - b)}{(b_o - b)}\, db. \tag{A6}$$

In (26) of the main text we showed that the flow in a rough fracture may be written as

$$Q(\Delta V) = Q(0)\, \frac{\langle b^3(\Delta V)\rangle}{\langle b^3(0)\rangle} = Q(0)\, \frac{\int_{\Delta V}^{b_o} n(b)s(b)(b - \Delta V)^3 db}{\int_0^{b_o} n(b)s(b)b^3 db}. \tag{A7}$$

Suppose we allow n(b)s(b) to vary as a power of aperture, obeying the normalization condition of (A4), then

$$n(b)s(b) = A\beta \left(\frac{b}{b_o}\right)^{\beta-1} \tag{A8}$$

where β is a dimensionless parameter. Given any value of β, one can put (A8) into (A6) and (A7) and compute the stress $\sigma(\Delta V)/E$ and the flow $Q(\Delta V)/Q(0)$, each in terms of the parameter $\Delta V/b_o$. The actual value of b_o is not known. Furthermore, the fractional contact area ω of all the asperities at any displacement ΔV can be determined from (A8),

$$\omega = \frac{\int_0^{\Delta V} n(b)s(b)db}{\int_0^{b_o} n(b)s(b)db} = \left(\frac{\Delta V}{b_o}\right)^{\beta}. \qquad \text{(A9)}$$

We now have the quantities $Q(\Delta V)/Q(0)$, $\sigma(\Delta V)/E$, and ω all in terms of $\Delta V/b_o$ and β. We may choose to treat β as an adjustable parameter to calculate curves of flow versus stress. Then the β determined from such a procedure will also dictate the theoretical fractional contact area ω at any specified displacement ΔV. Conversely, if one chooses to specify the value of ω, we are in fact fixing β, and this value of β from (A9) will determine the variation of flow versus stress. Both procedures were employed in the analysis of Iwai's (1976) flow and stress-displacement data.

ACKNOWLEDGEMENT

We would like to thank Professor Neville G. W. Cook for discussions in the initial phases of this work. This work is supported by the Department of Energy under contract W-7405-ENG-48.

REFERENCES

Bear, J., Dynamics of Fluids in Porous Media, Elsevier, New York, 1972.

Boussinesq, J., Jour. de Liouville, 13, 377-424, 1868.

Gangi, A. F., Variation of whole and fractured porous rock permeability with confining pressure, Int. J. Rock Mech. Min. Sci., 15, 249-257, 1978.

Goodman, R. E., The mechanical properties of joints. Proceedings of the Third Congress, International Society for Rock Mechanics, Denver, V.I-A, 1974.

Goodman, R. E., Method of Geological Engineering in Discontinuous Rocks. West Publishing Co., New York, 1976.

Iwai, K., Fundamental Studies of the Fluid Flow Through a Single Fracture. Ph.D. thesis, U. of California, Berkeley, 1976.

Kranz, R. L., Frankel, A. D., Engelder, T., and Scholz, C. H., The permeability of whole and jointed Barre granite. Int. J. Rock. Mech. Min. Sci., 16, 225-234, 1979.

Lomize, G. M., Filtratsiya V Treshchinovatykh Porodakh (Flow in Fractured Porous Rocks), Gosenergoizdat, Moscow, 1951.

Louis, C., A study of groundwater flow in jointed rock and its influence on the stability of rock masses. Imperial College Rock Mechanics Research Report No. 10, 1969.

Nelson, R., Fracture Permeability in Porous Reservoirs: Experimental and Field Approach. Ph.D. Dissertation, Department of Geology, Texas A&M University, 1975.

Ohnishi, Y., Laboratory Measurement of Induced Water Pressures in Jointed Rock. Ph.D. Thesis, U. of California, Berkeley, 1973.

Romm, E. S., Filtratsionnye Svoistva Treshchinovatykh Gornyx Porod (Flow Characteristics of Fractured Rocks). Nedra, Moscow, 1966.

Snow, D. T., A Parallel Plate Model of Fractured Permeable Media. Ph.D. thesis, U. of California, Berkeley, 1965.

Walsh, J. B., The effect of cracks on the uniaxial elastic compression of rocks. J. Geophys. Res., 70, 399-411, 1965.

Witherspoon, P. A., Wang, J. S. Y., Iwai, K., and Gale, J. E., Validity of cubic law for fluid flow in a deformable rock fracture. Water Resour. Res. 16(6), 1016-1024, 1980.

NOMENCLATURE

a	typical asperity size	L
A	fracture cross sectional area	L^2
b	fracture aperture	L
b_o	maximum fracture aperture	L
b_r	residual fracture aperture	L
C	constant in cubic flow law	
d	crack length	L
E	Young's modulus for rock	M/LT^2
E_{eff}	Effective Young's modulus for jointed rock	M/LT^2
f	size-effect factor	
g	acceleration of gravity	L/T^2
h	asperity height in fracture	L
ΔH	piezometric head	
j	summation index	
k_j	spring constant of the j^{th} asperity	M/T^2
ℓ	length over which displacement measurements are made	L
L	length of rectangular rock sample	L
M	number of voids in schematic representation of fracture	
$n(h)dh$	asperity height distribution function	
$N_c(\Delta V)$	number of areas of contact in fracture	
Q	flow rate	L^3/T
r_e	outer radius of cylindrical sample	L
r, θ, z	cylindrical coordinates	

r_w	wellbore radius of cylindrical sample	L
s_j	cross section area of the j^{th} asperity	L^2
u	volume enclosing one crack	L^3
U	equivalent flow velocity	L/T
$\vec{v}$	flow velocity	L/T
Δv	fracture deformation	L
Δv_r	rock deformation	L
Δv_m	maximum value of measured fracture deformation	L
Δv_t	total jointed rock deformation	L
W	width of rectangular sample	L
x, y, z	Cartesian coordinates	
$\hat{x}$, $\hat{y}$, $\hat{z}$	unit vectors	
α, β	parameters in analytical form of $N_c(\Delta v)$	
μ	dynamic fluid viscosity	M/LT
ρ	fluid density	M/L^3
σ	stress normal to fracture	M/LT^2
ω	contact area as a fraction of the total area of the fracture	

LIST OF FIGURES

12. Flow as a function of normal stress in basalt. (XBL 8011-2984)

13. Flow as a function of normal stress in marble. XBL 8011-2986)

14. Effect of repeated loading on the fracture deformation measurements in granite. (XBL 8011-2966)

15. Fracture roughness profile derived from "asperities in contact" function for granite and basalt. The insert of the cylindrical sample is there to indicate that the profile shown represents only a very small portion of the fracture. Note also the vertical scale enlargement over the horizontal scale. (XBL 8011-2987)

16. Theoretical flow as a function of stress in the first loading and unloading cycles in granite. (XBL 8011-2989)

17. Theoretical flow as a function of stress in the repeated loading and unloading cycles in granite. (XBL 8011-2990)

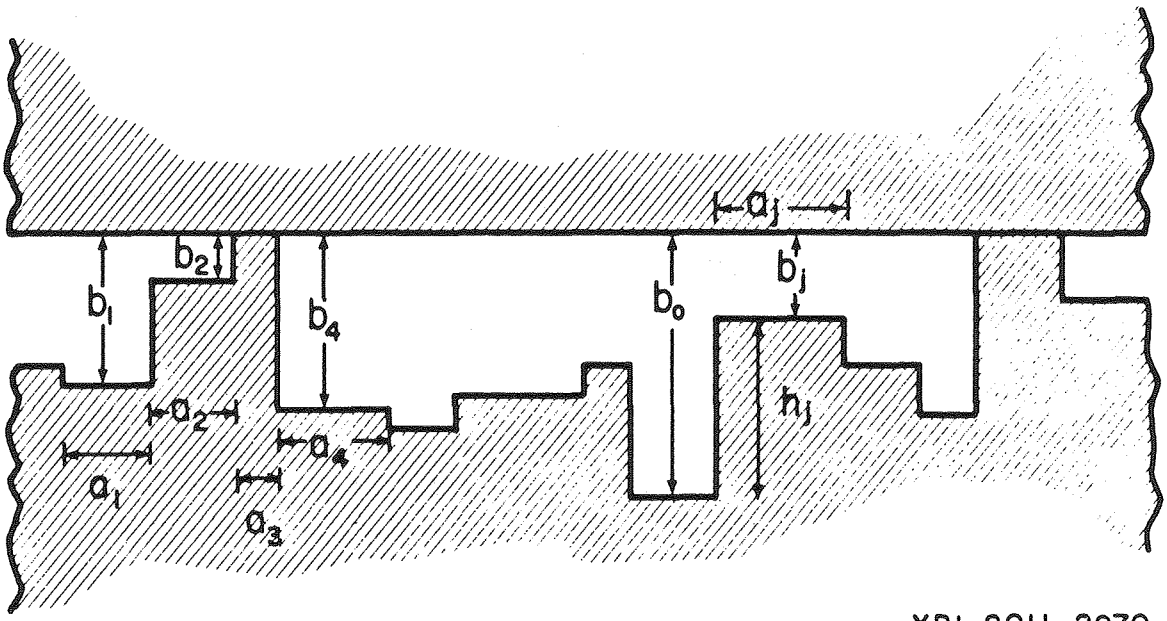

XBL 8011-2970

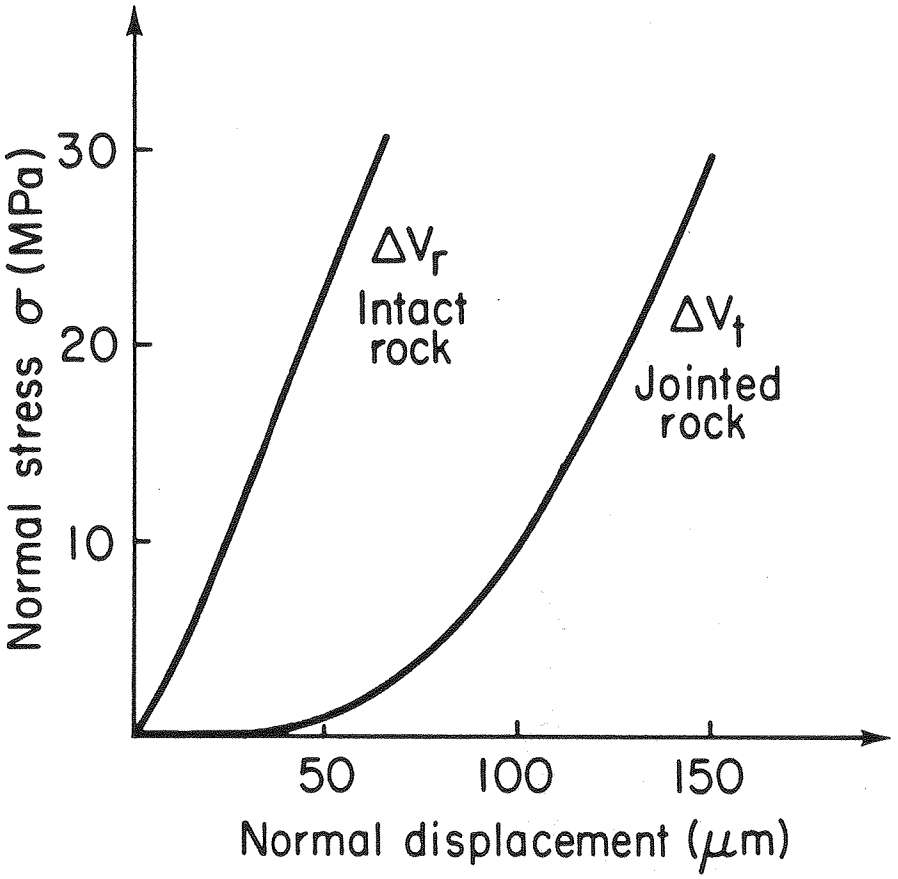

XBL 8011-2971

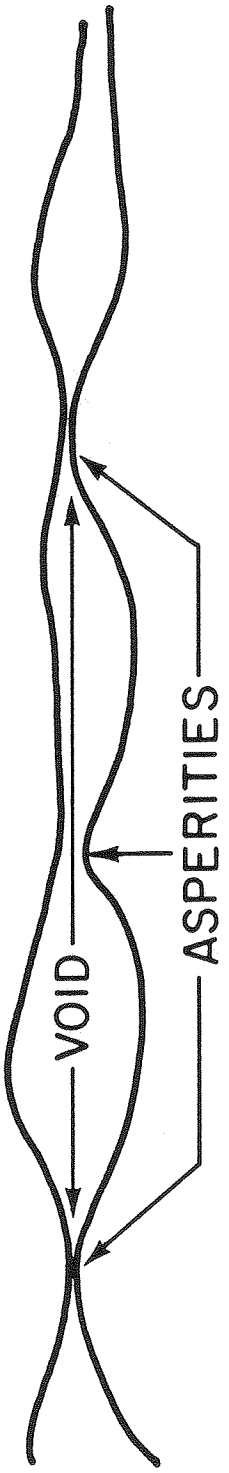

XBL 8011-2972

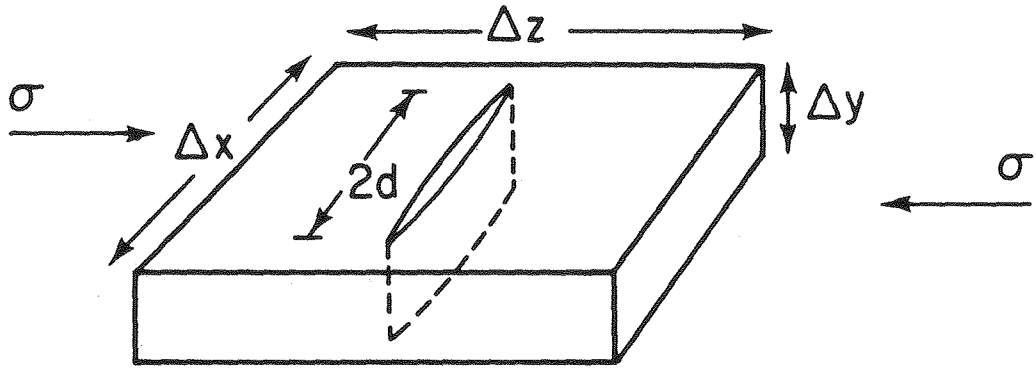

XBL 8011-2973

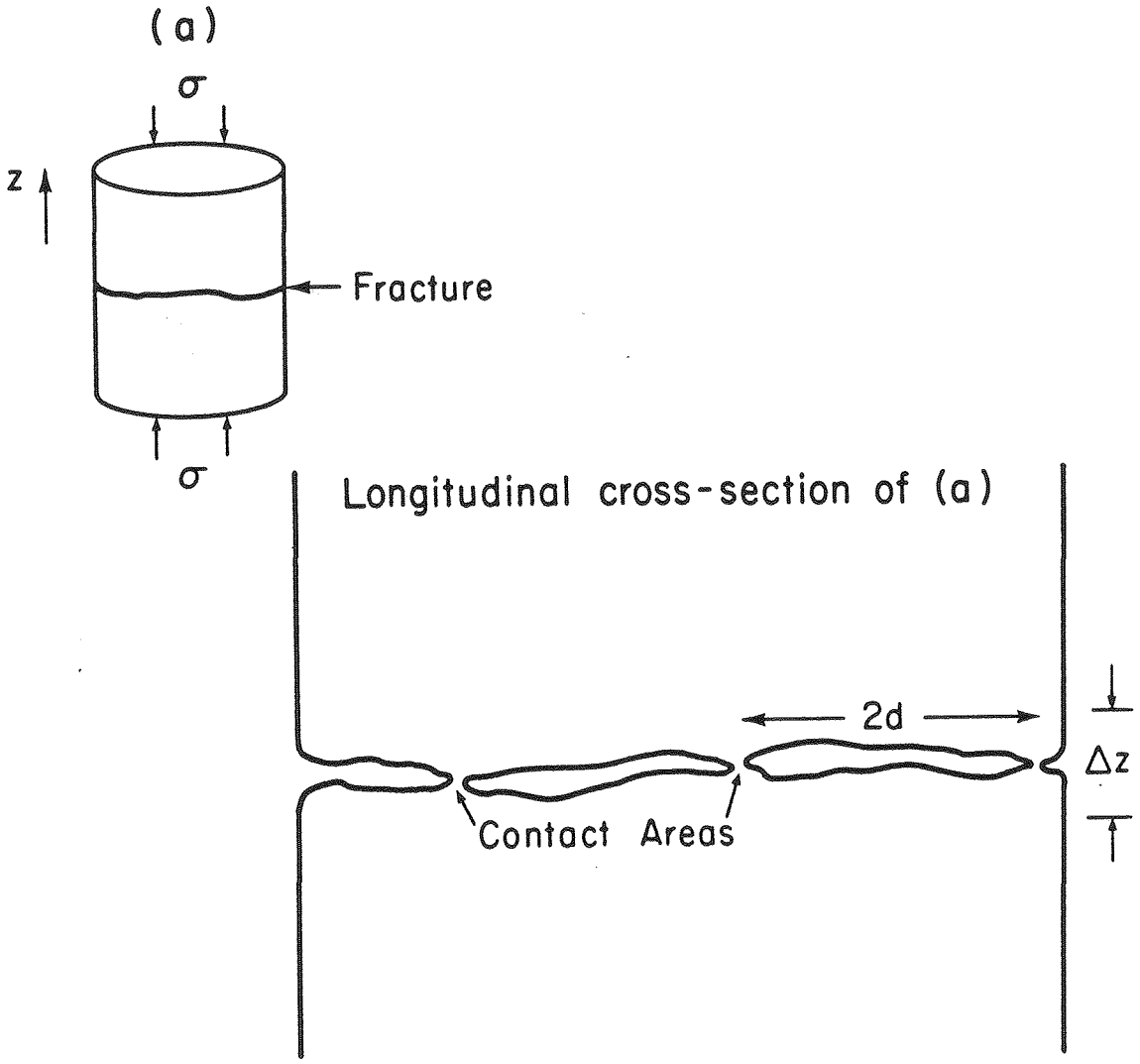

XBL 8011-2974

(a) at normal stress σ_1

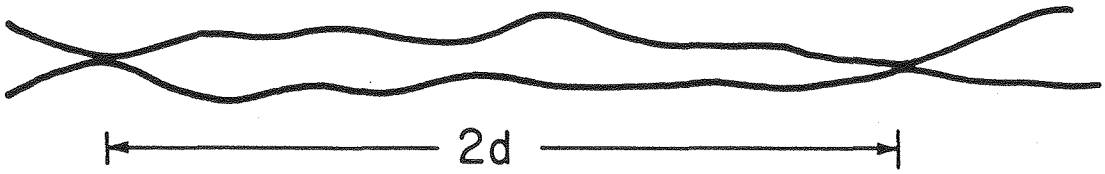

(b) at normal stress $\sigma_2 > \sigma_1$

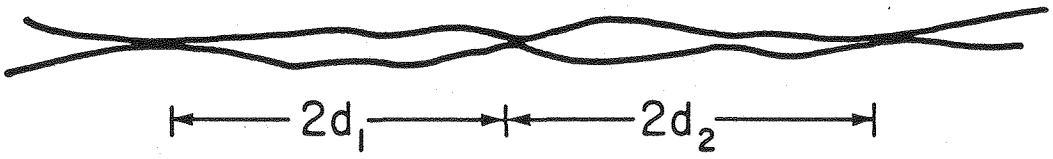

(c) at normal stress $\sigma_3 > \sigma_2$

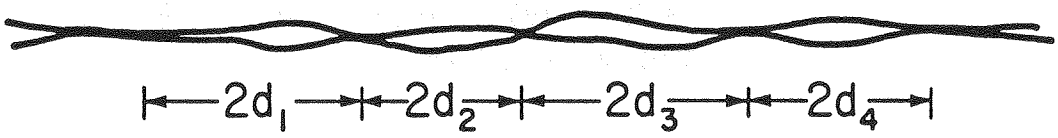

XBL 8011-2975

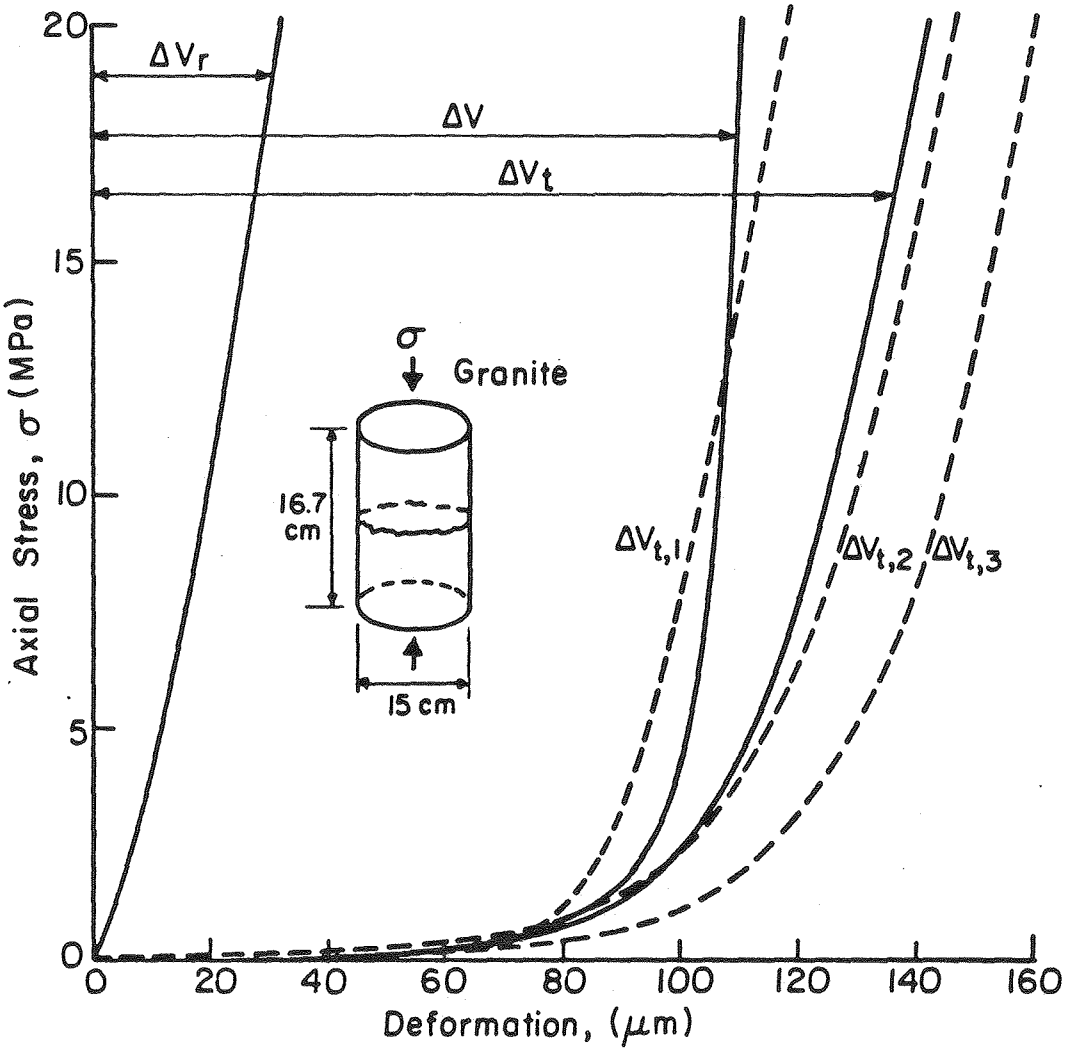

XBL 8011-2965

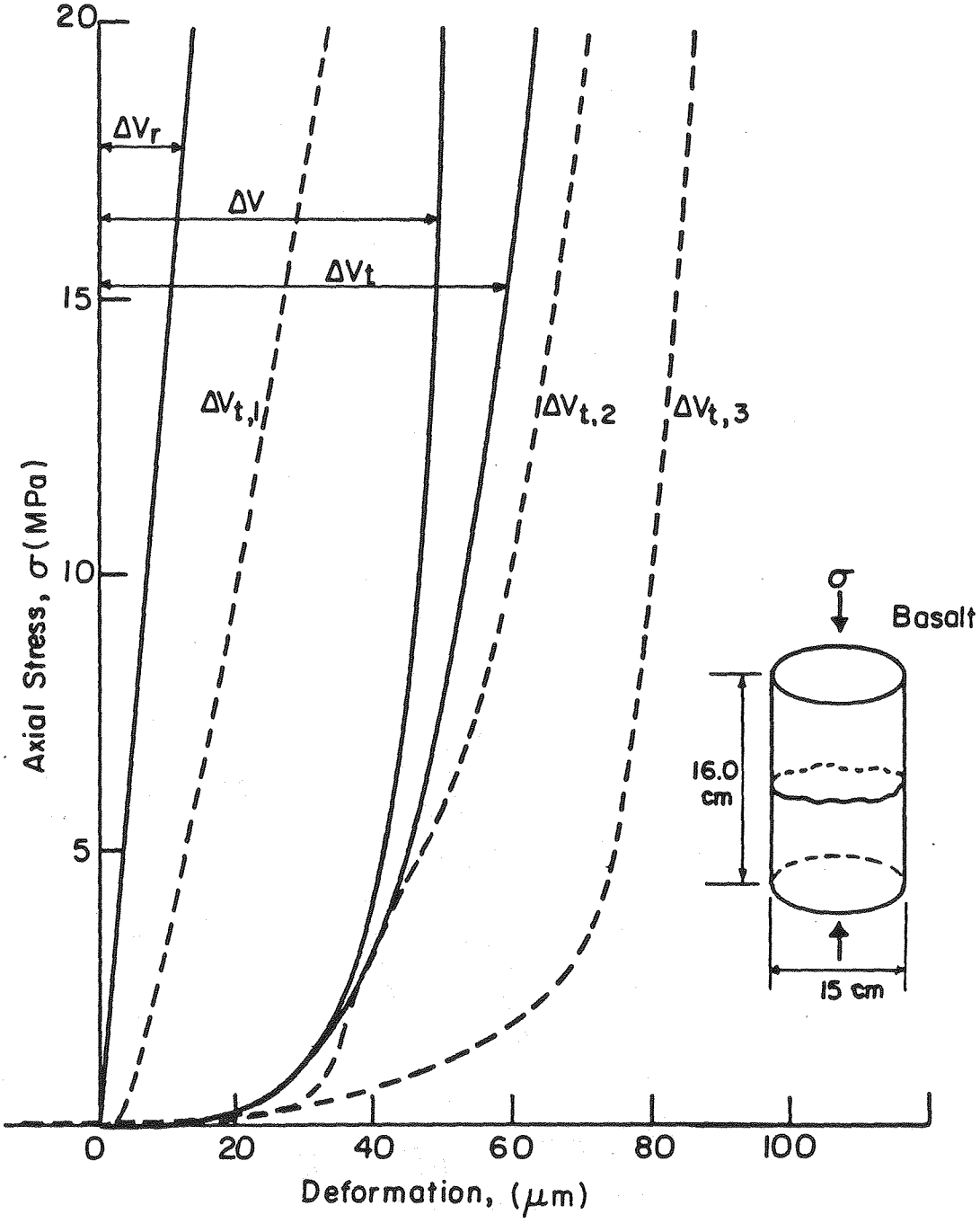

XBL 8011-2967

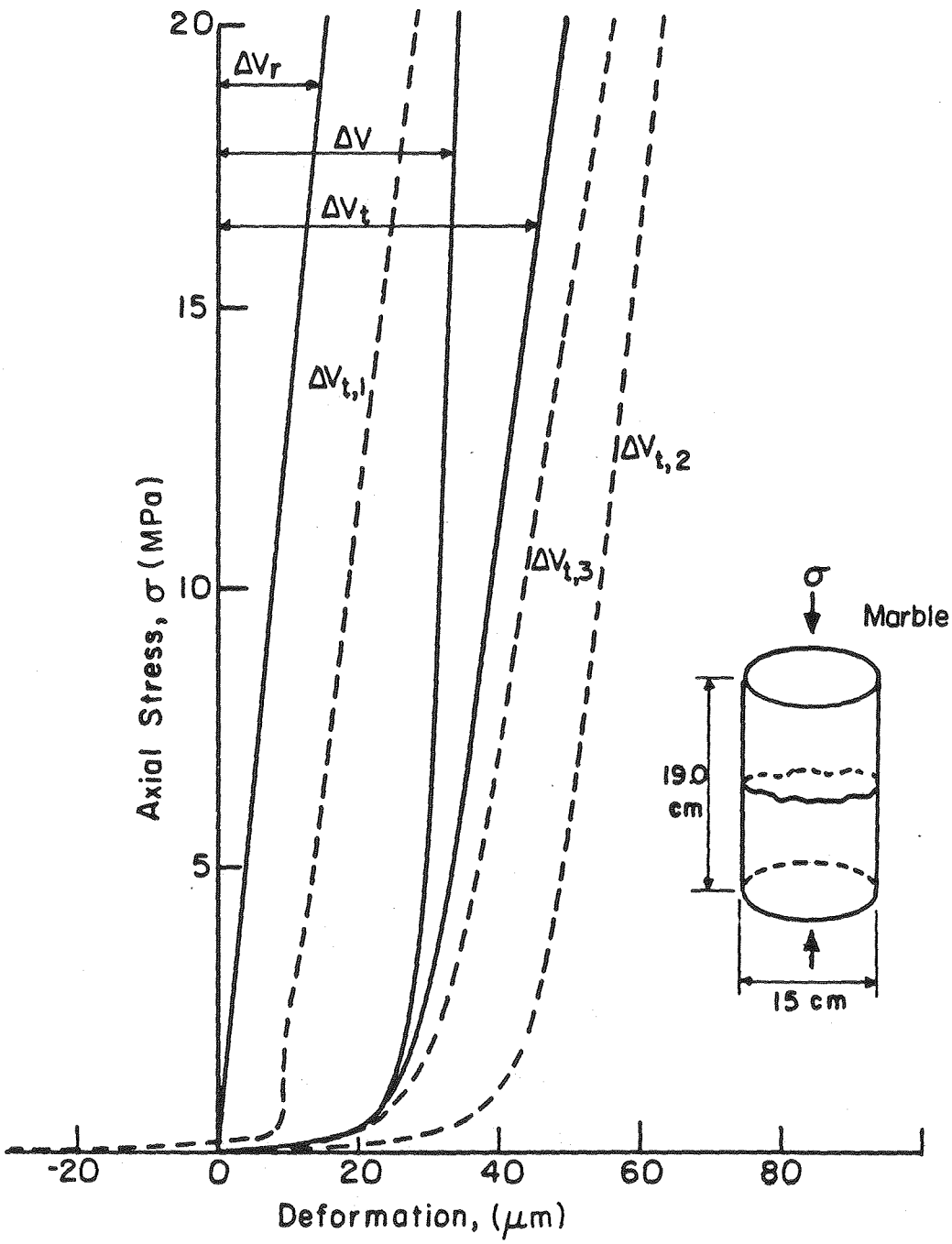

XBL 8011-2969

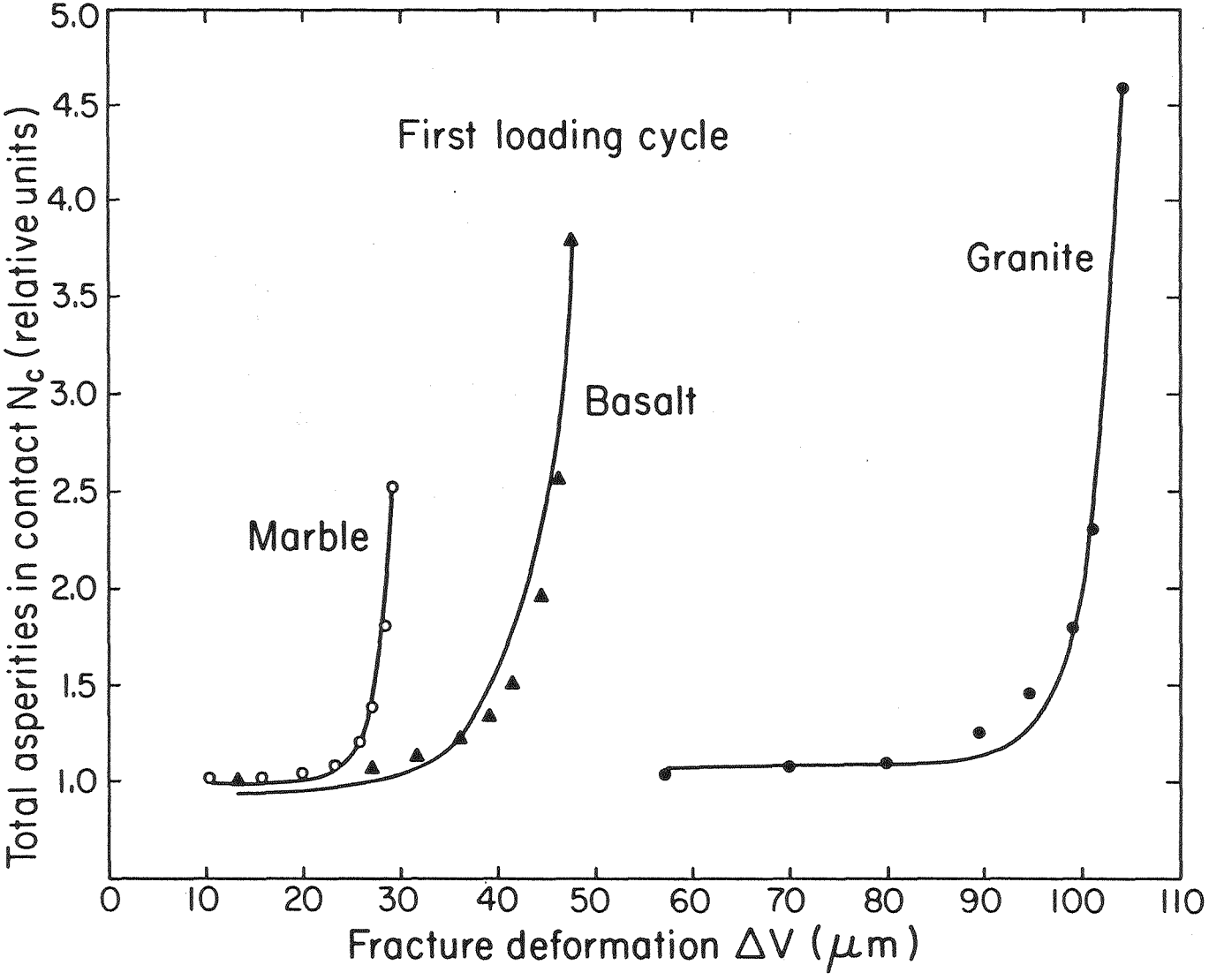
First loading cycle
Granite
Basalt
Marble
Total asperities in contact N_c (relative units)
Fracture deformation ΔV (μm)
5.0
4.5
4.0
3.5
3.0
2.5
2.0
1.5
1.0
0
10
20
30
40
50
60
70
80
90
100
110
XBL 8012-6565

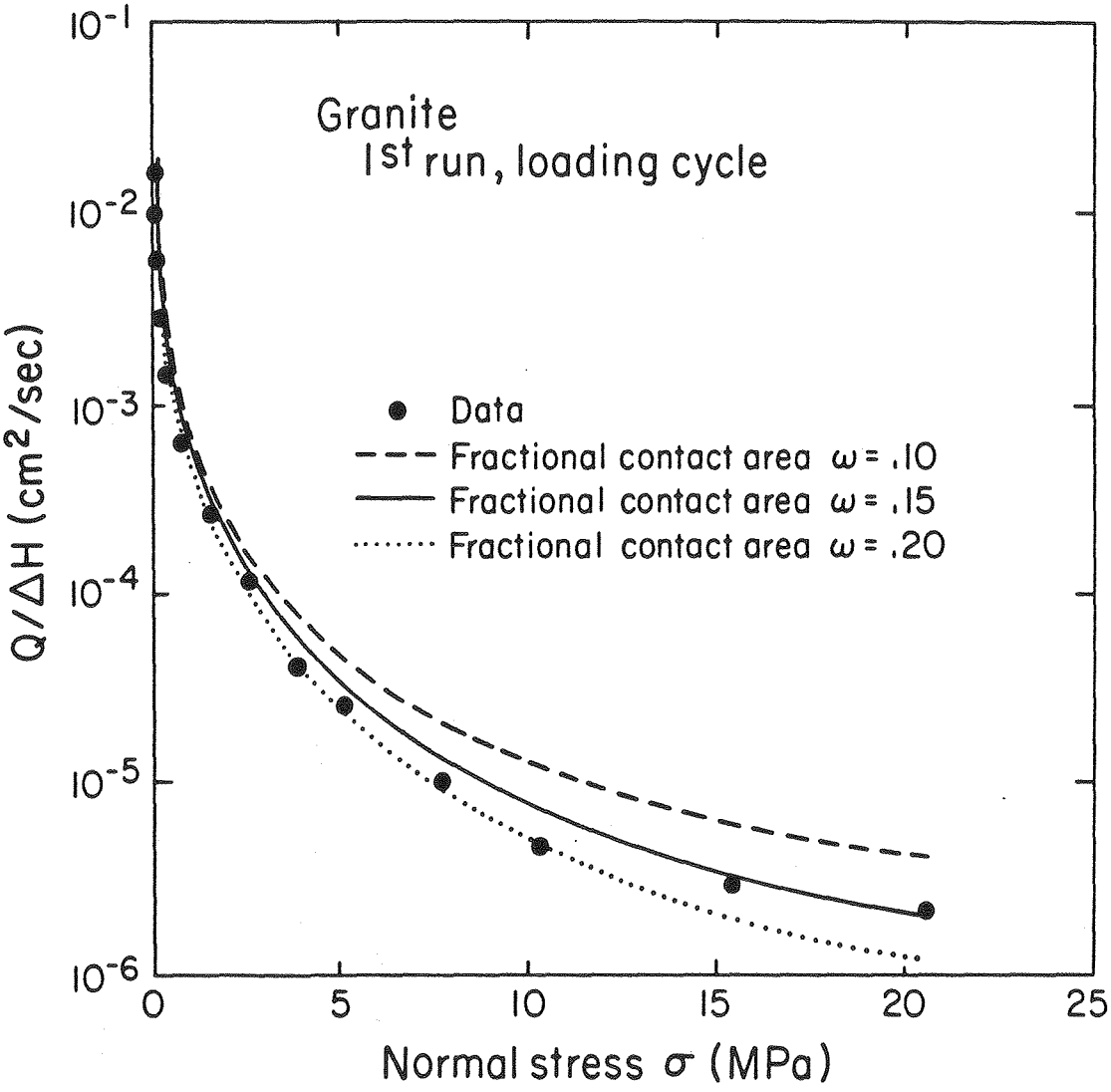
Granite
1st run, loading cycle
Data
Fractional contact area ω = .10
Fractional contact area ω = .15
Fractional contact area ω = .20
Q/ΔH (cm²/sec)
Normal stress σ (MPa)
10⁻¹
10⁻²
10⁻³
10⁻⁴
10⁻⁵
10⁻⁶
0
5
10
15
20
25
XBL 8011-2983

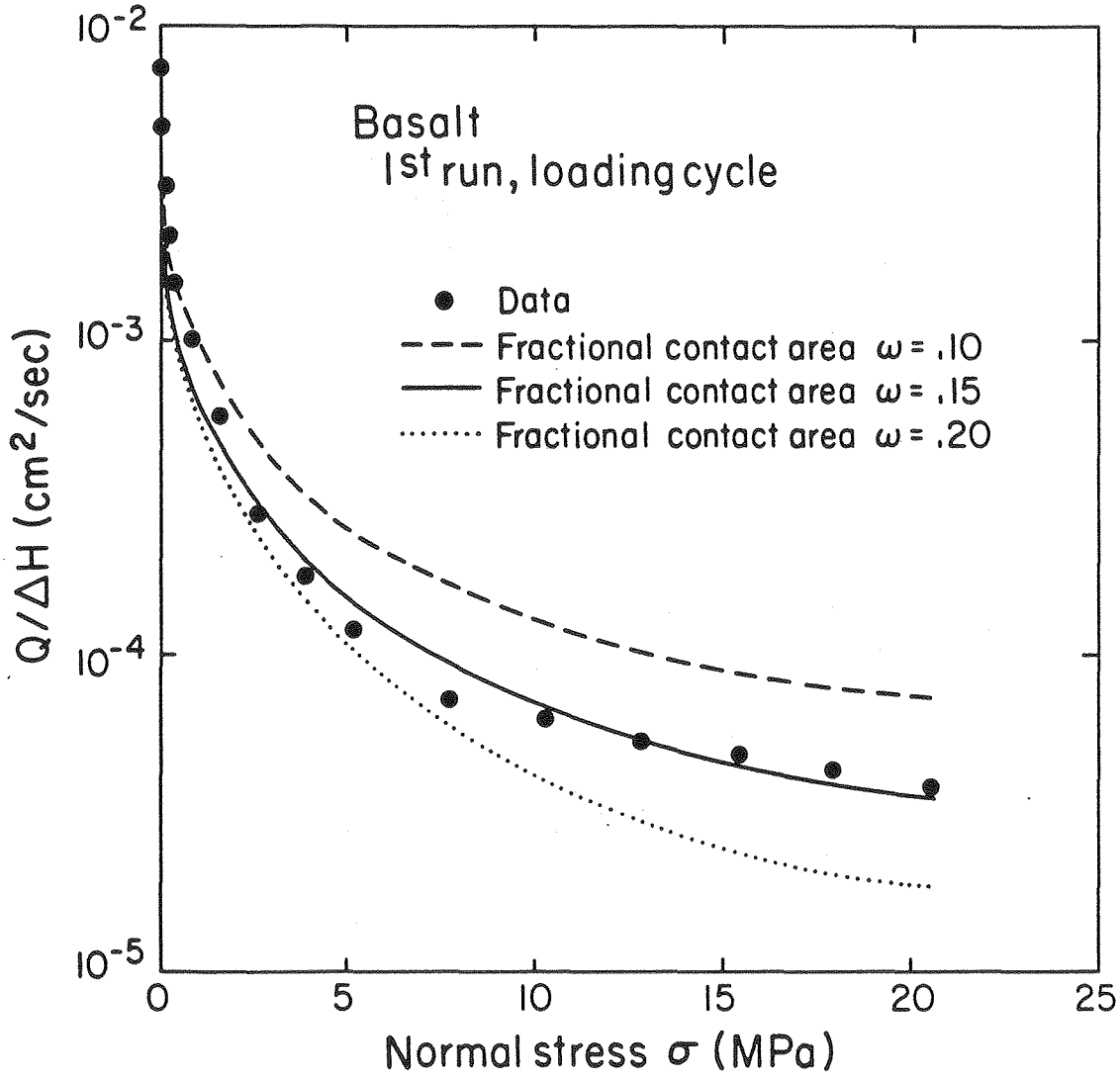

XBL8011-2984

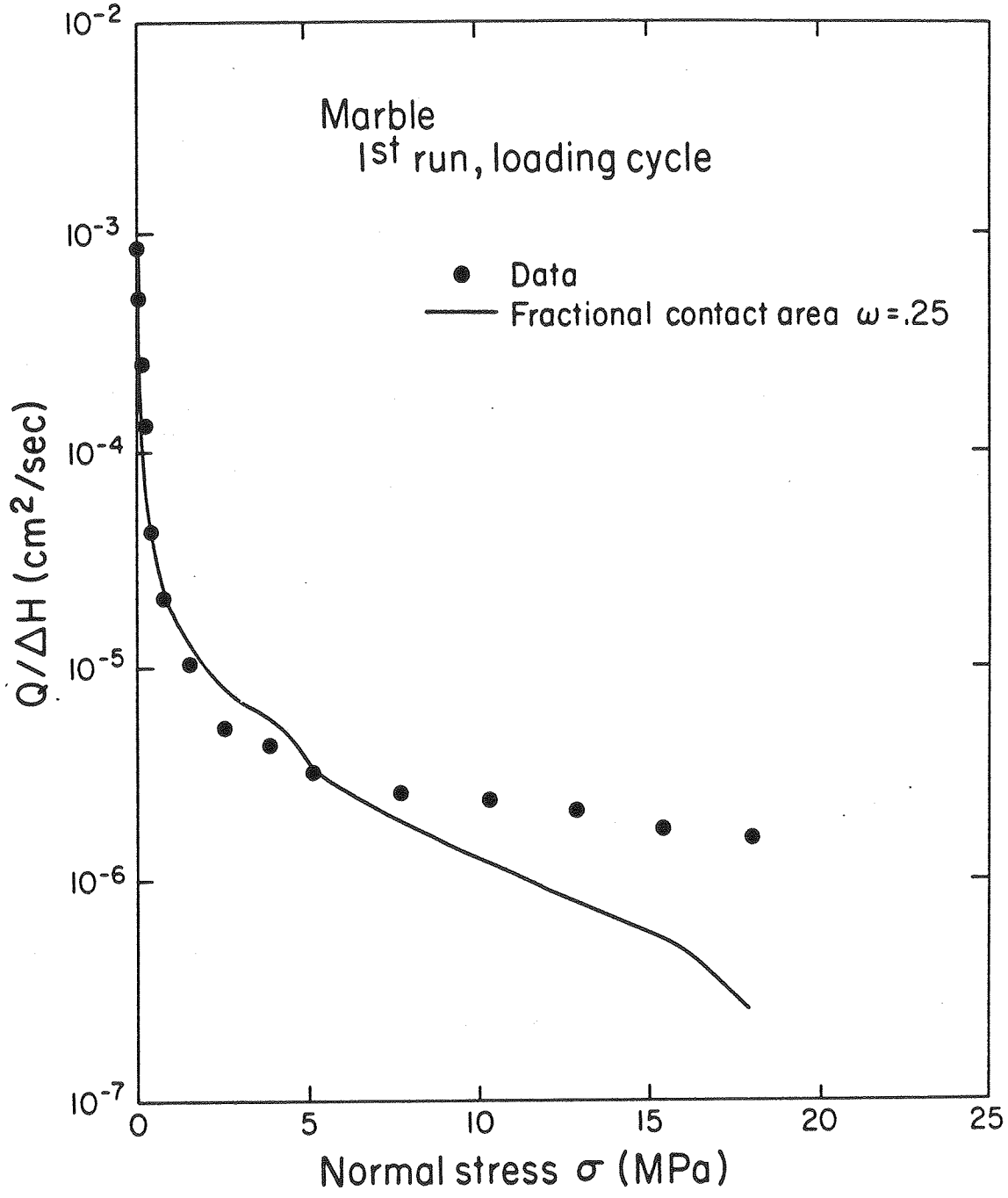
Marble
1st run, loading cycle
Data
Fractional contact area ω=.25
Q/ΔH (cm²/sec)
10⁻²
10⁻³
10⁻⁴
10⁻⁵
10⁻⁶
10⁻⁷
0
5
10
15
20
25
Normal stress σ (MPa)
XBL 8011-2986

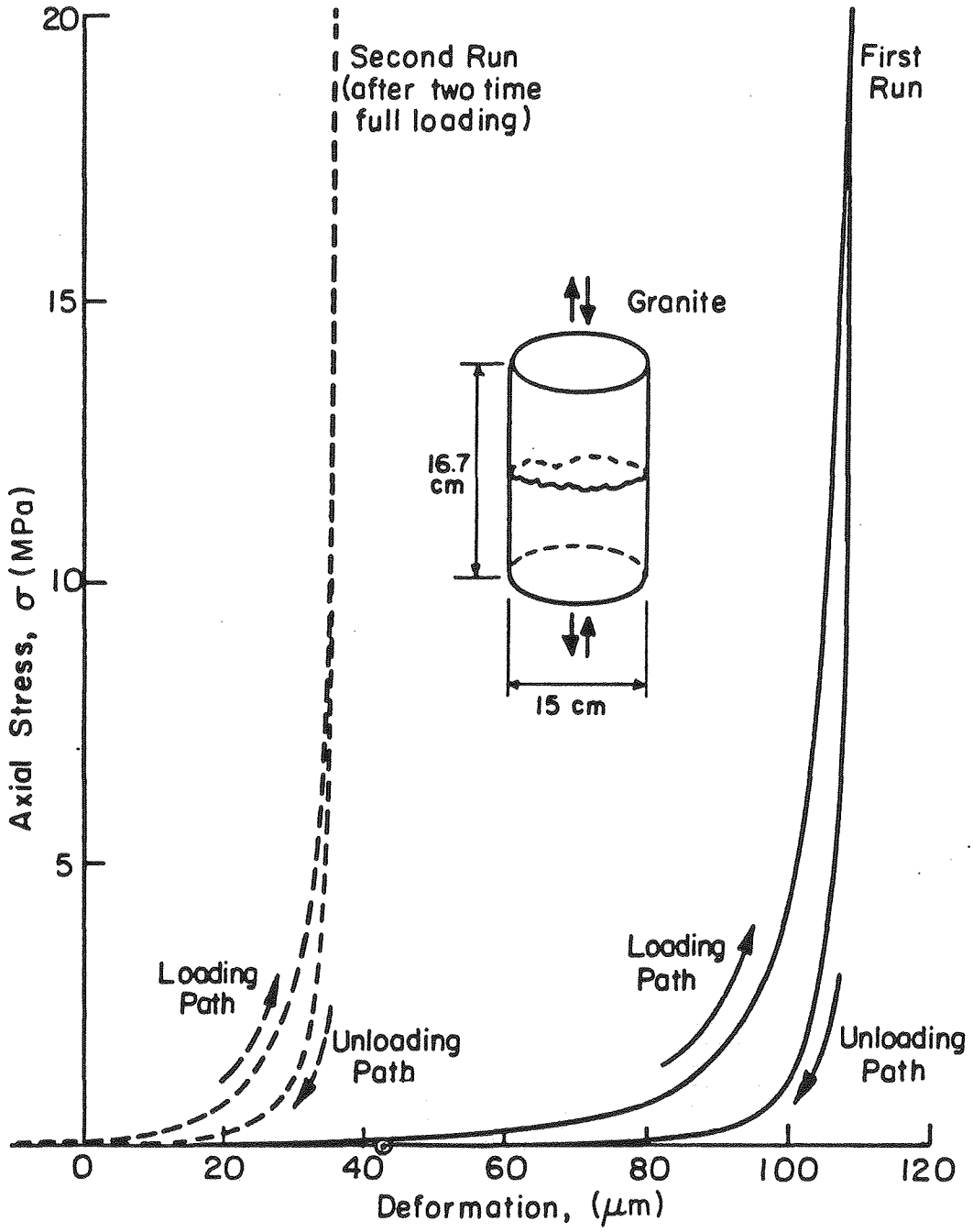

XBL 8011-2966

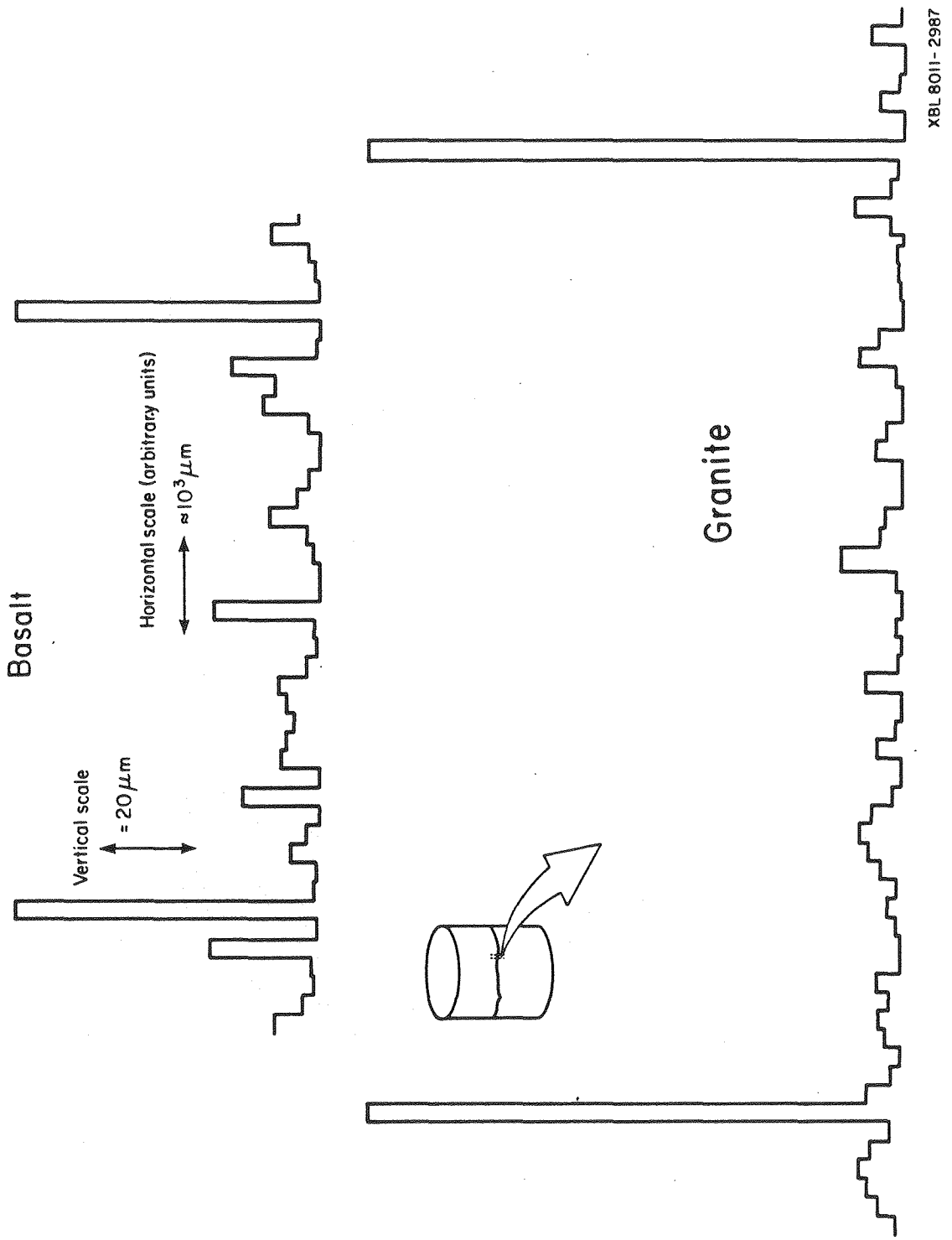
Basalt
Vertical scale
= 20 μm
Horizontal scale (arbitrary units)
≈ 10³ μm
Granite
XBL 8011-2987

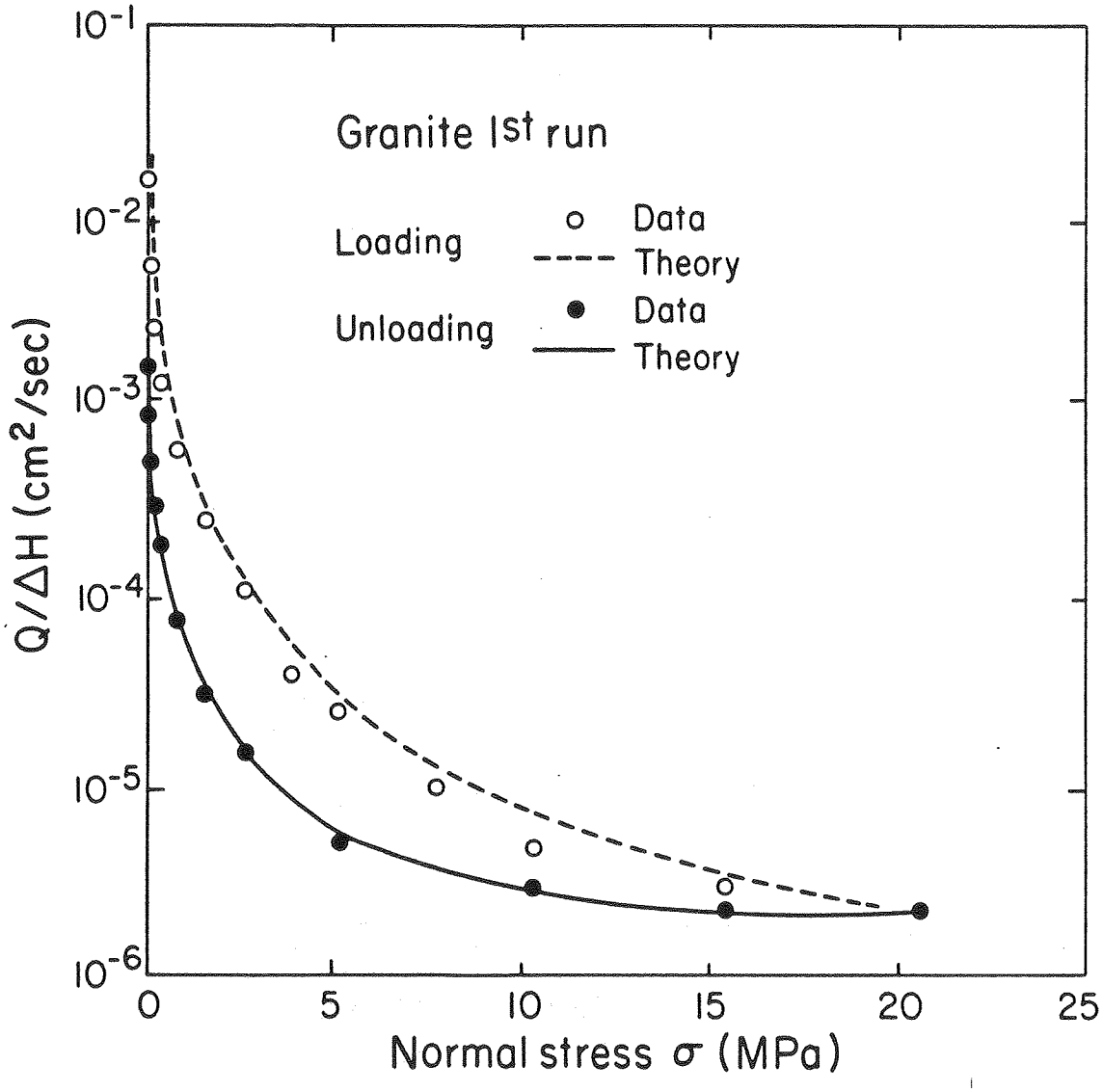

XBL 8011-2989

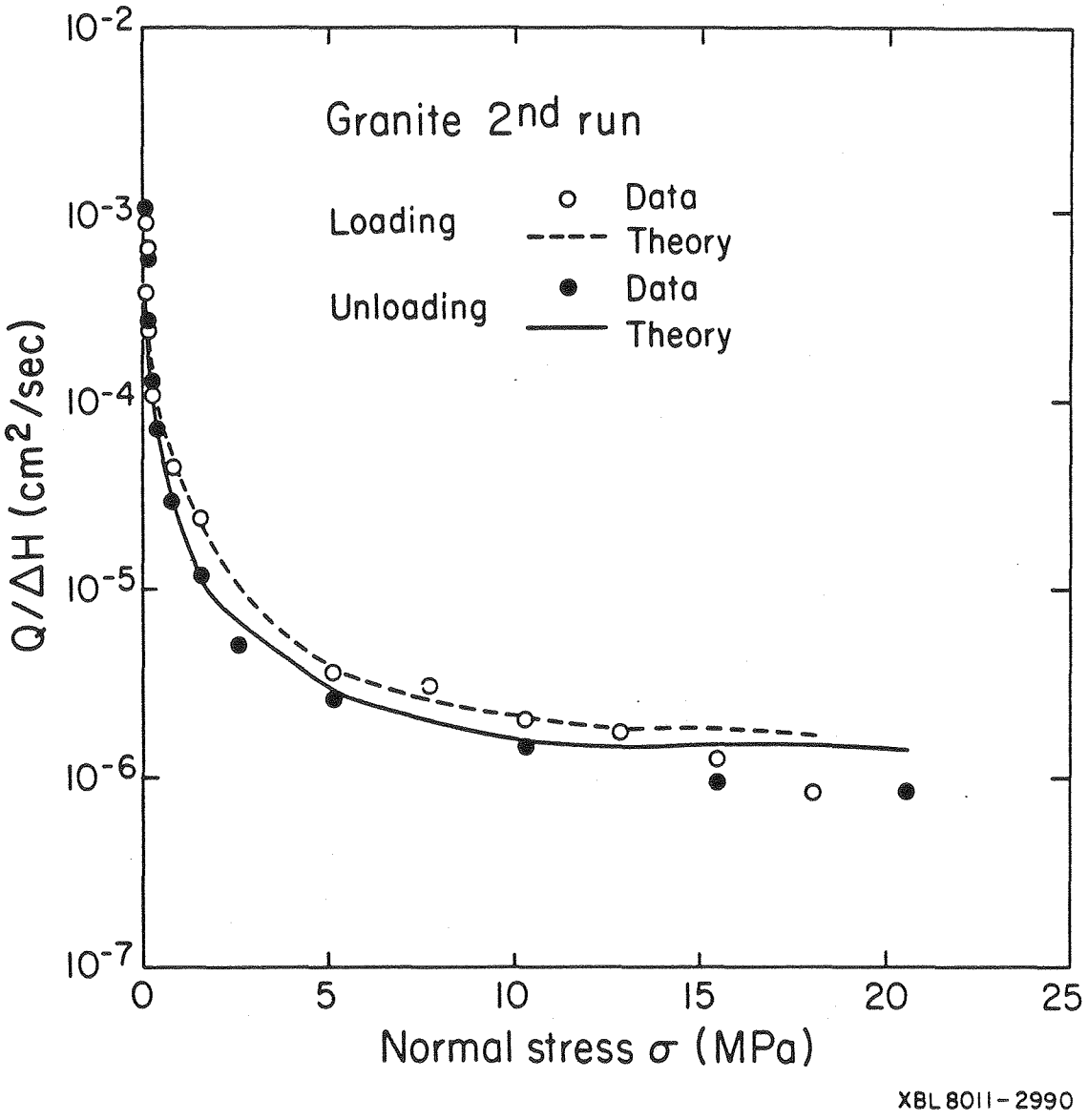
Granite 2nd run
Loading
Data
Theory
Unloading
Data
Theory
10^{-2}
10^{-3}
10^{-4}
10^{-5}
10^{-6}
10^{-7}
$Q/\Delta H$ (cm^2/sec)
0
5
10
15
20
25
Normal stress σ (MPa)
XBL 8011-2990